Structure, Magnetic Properties, Mössbauer and Catalase-like Activity of Spin Crossover Iron(III) Complexes with Salicylaldimine Ligands

Meichen Wang[a] (王美滇), Gene-Hsiang Lee[c] (李錦祥), Yu Wang[c] (王　瑜), Teng-Yuang Dong[b] (董滕永) and Ho-Hsiang Wei[a]* (魏和祥)

[a]*Department of Chemistry, Tamkang University, Tamsui, Taiwan, R.O.C.*

[b]*Department of Chemistry, Sun Yat-sen University, Kaohsiung, Taiwan, R.O.C.*

[c]*Department of Chemistry, National Taiwan University, Taipei, Taiwan, R.O.C.*

The preparation and characterization of three new spin-crossover ferric complexes with the composition $[Fe(5\text{-Br-Salmeen})_2]ClO_4$ (**1**), $[Fe(5\text{-Br-SalEen})_2]PF_6.CH_2Cl_2$ (**2**), and $[Fe(3\text{-}OCH_3\text{-Salpen})_2]PF_6$ (**3**), where substituted Salmeen, SalEen, and Salpen result from the Schiff-base condensation of substituted salicylaldehyde with N-methylethylenediamine, N-ethylethylenediamine, and N-methylpropylenediamine, respectively. The structural determinations reveal that complexes **1**-**3** cations possess the same general structure with the N_4O_2 donor atom set from two tridentate ligands forming a distorted octahedron about the Fe(III) ion. Complexes **1**-**3** have been shown by variable-temperature magnetic susceptibility (2-300 K) and ^{57}Fe Mössbauer spectroscopy to be (low-spin, S = 1/2) $\leftrightarrow$ (high-spin, S = 5/2) spin-equilibrium compounds in the solid state. The H_2O_2 disproportionation of complexes **1**-**3** in methanol at 25 °C show the rate law of $k_{obs}[H_2O_2][complex]$.

INTRODUCTION

Catalases catalyze the disproportionation of hydrogen peroxide to dioxygen and water, $H_2O_2 \rightarrow H_2O + 1/2\ O_2$, protecting cells against damage. Although most catalases contain the heme type mononuclear iron(III)-protoporphyrin IX prosthetic group,[1] recently, several synthetic oxo-bridged diiron(III) complexes showed catalase-like and oxygenation activity,[2-3] in which it has been assumed that an active species may be a μ-oxo diiron(III) species in these catalase-like activities of binuclear iron(III) compounds. Recently, we have reported that oxo-bridged binuclear iron(III) complexes with substituted salicylaldimine ligands have shown high catalase-activity with a reaction rate of $k[H_2O_2]^2$ [complex].[4] To extend our research vision on the model metal-complexes having catalase-activity, here we deal with the mono nuclear iron(III) complex with substituted salicylaldimine ligands (see Scheme I). The mono nuclear Iron(III) complexes with substituted salicylaldimine ligands have been investigated as model catechol dioxygenases; however, they have not been dealt with as a catalase-like model complex.

It is well known that several mono nuclear iron(III) complexes with substituted salicylaldimine ligands exhibit properties characteristic of "spin-equilibrium or spin crossover" complexes, where a high-spin (S = 5/2) excited state is within the thermal energy of the low-spin (S = 1/2) ground state.[5-11] The situation of spin crossover is dependence of the ligand field strength of iron(III) complexes, in which the substituent in salicylaldimine ligand plays an important role on tuning the ligand field strength. We chose these spin crossover iron(III) complexes with salicylaldimine ligands first to deal with their catalase-like activity in methanol solution. Here we prepared new four iron(III) complexes, $[Fe^{III}(5\text{-Br-Salmeen})_2]ClO_4$ (**1**), $[Fe^{III}(5\text{-Br-SalEen})_2]PF_6.CH_2Cl_2$ (**2**),

Scheme I

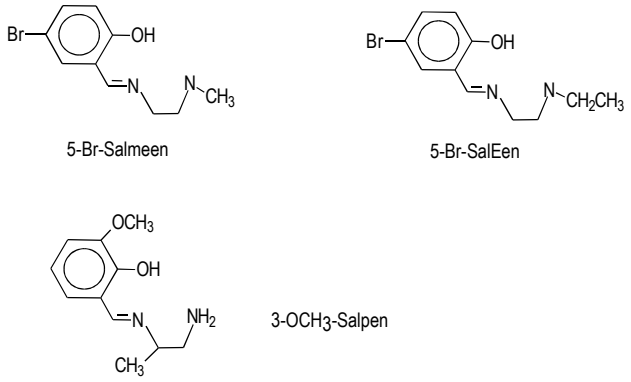

Dedicated to the celebration of the seventieth anniversary of Chemical Society the located in Taipei.

* Corresponding author. E-mail: tkwei@mail.tku.edu.tw

and $[Fe^{III}(3\text{-}OCH_3\text{-}Salpen)_2]PF_6$ (**3**) where substituted 5-Br-Salmeen, 5-Br-SalEen, and 5-Br or 3-OCH_3-Salpen result from the Schiff-base condensation of substituted salicylaldehyde with N-methylethylenediamine, N-ethylethylenediamine, and N-methylpropylenediamine, respectively. The X-ray crystallographic analysis, ^{57}Fe-Mössbauer, Uv-vis, EPR, magnetic susceptibility, and H_2O_2 decomposition for complexes **1**-**3** are investigated.

EXPERIMENTAL

The ligands used in this study result from the Schiff-base condensation of substituted salicylaldehyde with N-methylethylenediamine, N-ethylethylenediamine, and N-methylpropylenediamine in methanol; they are abbreviated as 5-Br-Salmeen, 5-Br-SalEen, or 5-Br-SalEen, respectively (see Scheme I).

The complexes $[Fe(5\text{-}Br\text{-}Salmeen)_2]ClO_4$ (**1**), $[Fe(5\text{-}Br\text{-}SalEen)_2]PF_6.C_2H_2Cl_2$ (**2**), and $[Fe^{III}(3\text{-}OCH_3\text{-}Salpen)_2]PF_6$ (**3**) were obtained according to the general methods.[5-7] A methanol solution containing anhydrated $FeCl_3$, $NaClO_4$ or $NaPF_6$, and the ligand was refluxed for 1-2 h and the desired iron(III) complexes of **1**, **2** , and **3** were obtained and filtered off. The products were recrystallized from CH_2Cl_2 to give single crystals of complexes **1**-**3** suitable for X-ray crystallographic analysis. Anal. Calc.: for $C_{20}H_{22}ClBr_2FeN_2O_6$ (**1**): C, 35.14; H, 3.54; N, 8.19. Found: C, 35.30; H, 3.63, N, 8.17%. IR (KBr disc): ν(C=N), 1626(s) cm^{-1}. Calc.: for $C_{23}H_{28}Cl_2Br_2F_6FeN_4O_2P$ (**2**): C, 32.86; H, 3.59; N, 6.65. Found: C, 32.70; H, 3.63, N, 6.88%. IR (KBr disc): ν(C=N) 1629 cm^{-1}. Calc.: for $C_{22}H_{26}F_6FeN_4O_4$ P (**3**): C, 41.99; H,4.48; N, 8.90. Found: C, 41.67; H, 4.57; N, 8.74%. IR (KBr, disc): ν(C=N), 1624 (s) cm^{-1}.

Physical Measurements

IR spectra were recorded on a Bio-Rad FTS-40 FTIR spectrophotometer as KBr pellets in the 4000-400 cm^{-1} region. UV-VIS absorption spectra were recorded on a Cintra 20 spectrophotometer, X-band ESR spectra at 78 K for the complexes as powders on a Bruker ESC-106 spectrometer. Mössbauer effect measurements were carried out using an ASA-600 spectrometer with ^{57}Co(Rh) source. All velocity scales and isomer shifts refer to iron foil at 298 K. The temperature dependence of magnetic susceptibility was measured on a MPMS Quantum Design SQUID magnetometer in the range 2-300 K. Diamagnetic corrections were made using Pascal constants.[12]

X-ray Crystal Structure Analysis

Crystallographic data at 150 K of compounds **1-3** were collected on an Enraf-Nonius CAD4 four-circle diffractometer, and at 293 K for compounds **2** on a Siemens P4 diffractometer with graphite-monochromatized Mo K_α radiation (λ = 0.7107 Å), 2θ-θ scan mode. The N independent reflections and N_o with $I > 2.0\ \sigma(I)$ were observed. The structures were solved by direct method and refined (based on F^2) by a full-matrix least-squares method using the SHELXTL software package;[13] the function minimized was $\sum w(|F_o| - |F_c|)^2$ and unit weights were used. All non-hydrogen atoms were readily located and refined with anisotropic thermal parameters; $R_1 = \sum|F_o\text{-}F_c| / \sum|F_o|$ and $wR_2 = (\sum(w\ |F_o^2 - F_c^2|)^2 / |\sum w|F_o^2|^2)^{1/2}$ respectively. The summary of the crystal and diffraction data obtained at 150 K are given in Table 1, and the crystallographical data and experimental conditions of **2** at 293 K are deposited as supplementary. The selected bond distances and angles are given in Tables 2-3.

Hydrogen Peroxide Decomposition

The H_2O_2 dismutation activity and turnover were carried out by measuring the dioxygen evolution in methanol with a complex: H_2O_2 ratio of 1:400. All reactions were carried out at 25 °C in a 25 cm^3 reactor with stirring bar under air. Methanol (10 cm^3) was added to the complex (25 μmol, 0.2 mmol dm^{-3}) and pyridine (1 cm^3), then the flask was closed with a rubber septum. Hydrogen peroxide (1 cm^3, 30w/w (water) 10 m mol, 0.9 mmol dm^{-3}) was injected through the septum with a syringe. The reactor was connected to a graduated burette filled with water and dioxygen evolution was measured at time intervals during 10 s. by volumetry. The turnovers of the reaction at the first 60 min of complexes **1**, **2**, and **3** are 62, 71, and 56, respectively. Observed initial rates were expressed as mol dm^{-3} s^{-1} by taking the volume of the solution into account and calculated from the maximum slope of curves describing evolution of O_2 versus time. Plots of the initial rates versus the concentrations of H_2O_2 and iron(III) complexes **1**-**3** allowed determination of the reaction orders in both reactants. It should be noted that in the absence of pyridine the complexes were practically low active towards peroxide.

RESULTS AND DISCUSSION

Crystal Structures Description

The X-ray crystal structures determined at 150 K (without the solvent molecules and the anions) and atom number-

Table 1. Crystallographic Data for Complexes **1-3**

	1	**2**	**3**
Formula	$C_{20}H_{22}ClBr_2FeN_2O_6$	$C_{23}H_{28}Cl_2Br_2F_6FeN_4O_2P$	$C_{22}H_{26}F_6FeN_4O_4P$
M	665.54	824.03	611.29
Crystal system	monoclinic	monoclinic	triclinic
Space group	*P* 2_1/n	*P* 2_1/c	*P*$\bar{1}$
Unit cell dimensions			
a (Å)	10.9492(2)	10.8379(2)	9.4485(2)
b (Å)	24.9253(6)	28.6980(1)	10.5450(4)
c (Å)	18.7782(4)	11.0486(1)	13.1338(5)
α (°)			80.630(1)
β (°)		115.346(1)	79.979(2)
γ (°)			79.812(1)
Z	8	4	2
D_{calc} (g cm^{-1})	1.754	1.762	1.616
Crystal size (mm)	0.40 × 0.05 × 0.03	0.37 × 0.15 × 0.06	0.25 × 0.06 × 0.01
R_1	0.0524	0.0933	0.1089
wR_2	0.0934	0.2009	0.2414

Table 2. Selected Bond Distances (Å) and Angles (°) for Complex **1**

High-spin **1a**		Low-spin **1b**	
Fe-O(1)	1.934(4)	Fe'-O(1')	1.886(4)
Fe-O(2)	1.942(4)	Fe'-O(2')	1.896(4)
Fe-N(1)	2.207(5)	Fe'-N(1')	2.065(4)
Fe-N(2)	2.123(4)	Fe'-N(2')	1.957(5)
Fe-N(3)	2.209(5)	Fe'-N(3')	2.056(4)
Fe-N(4)	2.124(4)	Fe'-N(4')	1.952(4)
O(1)-Fe-N(1)	163.57(16)	O(1')-Fe'-N(1')	174.72(17)
O(2)-Fe-N(3)	163.40(16)	O(2')-Fe'-N(3)	174.40(17)
N(2)-Fe-N(4)	175.17(18)	N(2')-Fe'-N(4')	178.05(19)
O(1)-Fe-O(2)	96.84(18)	O(1')-Fe'-O(2')	95.28(17)
O(2)-Fe-N(2)	95.73(16)	O(2')-Fe'-N(2')	87.13(17)
O(1)-Fe-N(2)	85.88(17)	O(1')-Fe'-N(2')	92.73(18)
O(1)-Fe-N(4)	98.34(17)	O(1')-Fe'-N(4')	85.32(17)
O(2)-Fe-N(1)	89.50(17)	O(2')-Fe'-N(1')	87.74(17)
O(1)-Fe-N(3)	89.80(18)	O(1')-Fe'-N(3')	87.99(17)
N(2)-Fe-N(3)	99.92(17)	N(2')-Fe'-N(3')	97.27(18)
N(1)-Fe-N(3)	88.27(17)	N(1')-Fe'-N(3')	89.35(18)

Table 3. Selected Bond Distances (Å) and Angles (°) for **2** and **3** at 150 K

Complex **2**			
Fe-O(1)	1.912(6)	Fe-O(2)	1.914(7)
Fe-N(1)	2.116(8)	Fe-N(2)	1.991(8)
Fe-N(3)	2.126(7)	Fe-N(4)	1.999(7)
O(1)-Fe-N(1)	172.6(3)	O(2)-Fe-N(3)	172.9(3)
N(2)-Fe-N(4)	179.5(3)	O(1)-Fe-O(2)	94.6(3)
O(1)-Fe-N(2)	91.9(3)	O(2)-Fe-N(2)	88.3(3)
O(1)-Fe-N(4)	88.3(3)	O(2)-Fe-N(4)	92.2(3)
O(2)-Fe-N(1)	89.1(3)	O(1)-Fe-N(3)	88.8(3)
N(2)-Fe-N(1)	81.8(3)	N(1)-Fe-N(3)	88.2(3)
N(2)-Fe-N(3)	97.9(3)	N(3)-Fe-N(4)	81.7(3)
Complex **3**			
Fe-O(1)	1.876(6)	Fe-O(2)	1.849(6)
Fe-N(1)	2.015(7)	Fe-N(2)	1.911(7)
Fe-N(3)	1.992(8)	Fe-N(4)	1.921(8)
O(1)-Fe-N(1)	177.1(3)	O(2)-Fe-N(3)	176.0(3)
N(2)-Fe-N(4)	179.0(3)	O(1)-Fe-O(2)	94.5(3)
O(1)-Fe-N(2)	93.3(3)	O(2)-Fe-N(2)	86.6(3)
O(1)-Fe-N(4)	86.4(3)	O(2)-Fe-N(4)	94.4(3)
O(2)-Fe-N(1)	87.0(3)	O(1)-Fe-N(3)	89.0(3)
N(2)-Fe-N(1)	84.2(3)	N(1)-Fe-N(3)	89.6(3)
N(2)-Fe-N(3)	95.2(3)	N(3)-Fe-N(4)	83.9(3)

ing schemes for complexes **1**, **2**, and **3** are shown in Figs. 1, 2, and 3, respectively, while selected bond lengths and angles are listed in Tables 2-3. All of the structures illustrated that three cations possess the same general structure with an N_4O_2 donor atom set from two tridentate ligands forming a distorted octahedron about the Fe(III) ion. In each case the terminal oxygen atoms occupy *cis* positions and the remaining four nitrogen atoms, two *cis* amines and two trans imines, complete the coordination sphere iron.

As shown in Fig. 1, two crystallographically independent $[Fe(3\text{-}OCH_3\text{-}Salpen)_2]^+$ cations, characteristic of low-spin Fe(III) (**1b**) and high-spin Fe(III) (**1a**) forms, respectively, of complex **1** are present. The average bond distance of Fe-N (imine) (2.124(4) Å) of the high-spin Fe(III) is longer than that of Fe'-N'(imine) (1.955 (5) Å) of the low-spin Fe(III) form. It is well known that the average iron-donor atom distances in high-spin complexes are longer than those in low-spin complexes.[5,14-15]

Studies of the Schiff-base iron(III) complexes have shown that the metal to imine nitrogen bond distance is sensitive to the electronic spin state of the metal ion: the Fe-N(imine) distances are in the range ca. 2.00-2.10 Å for the high-spin state and in the range ca. 1.93-1.99 Å for the low-spin case.[14] In the structures of complexes **1-3** reported here the Fe-N(imine) bond distances of 2.124 (4) for **1a** at 150 K and 2.089 (10) Å for **2** at 293 K and 1.995 for **2** at 150 K, respectively, suggest that the Fe(III) ions are in a high-spin state. The Fe-N(imine) bond distances of 1.955 (5) for **1b**, 1.995 for **2** and 1.916 (8) for **3** at 150 K suggest that the Fe(III) ions in the complexes are in the low-spin state, which are consistent with the results of temperature-dependent magnetic susceptibility and Mössbauer effect measurements (see below).

The angles O(1)-Fe-N(1) and O(2)-Fe-N(3) for the high-spin **1a** (163.57(16)^o and 163.40(16)^o, respectively) deviate markedly from 180^o for an ideal octahedral; however, the angles O(1)-Fe-N(1) and O(2)-Fe-N(3) for the low-spin Fe(III) **1b** at 150 K (174.72 (17)° and 174.40 (17)°, respectively), for **2** at 150 K (and 172.6 (3)° and 172.9 (3)°, respectively), and for **3** (177.1 (3)° and 176.0 (3)°, respectively) are close to ideal octahedral 180°.

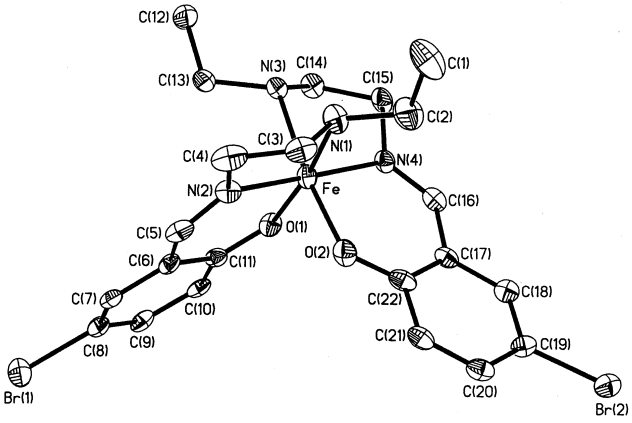

Fig. 2. Perspective view of complex **2** with the atom numbering scheme. The solvent CH_2Cl_2 and anion PF_6^- are omitted for clarity. Thermal ellipsoids are drawn at 50% probability level.

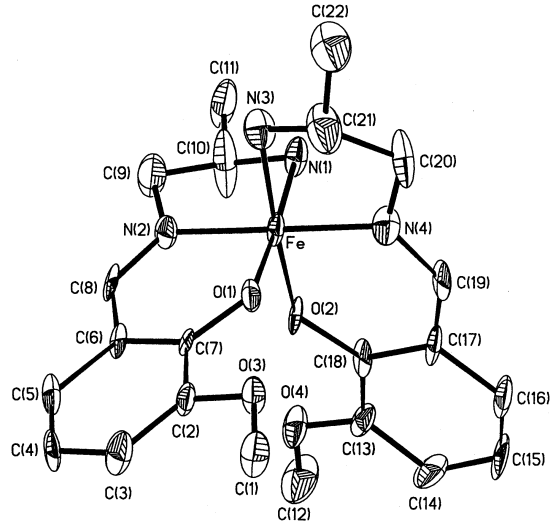

Fig. 3. Perspective view of complex **3** with the atom numbering scheme. The anion PF_6^- is omitted for clarity. Thermal ellipsoids are drawn at 50% probability level.

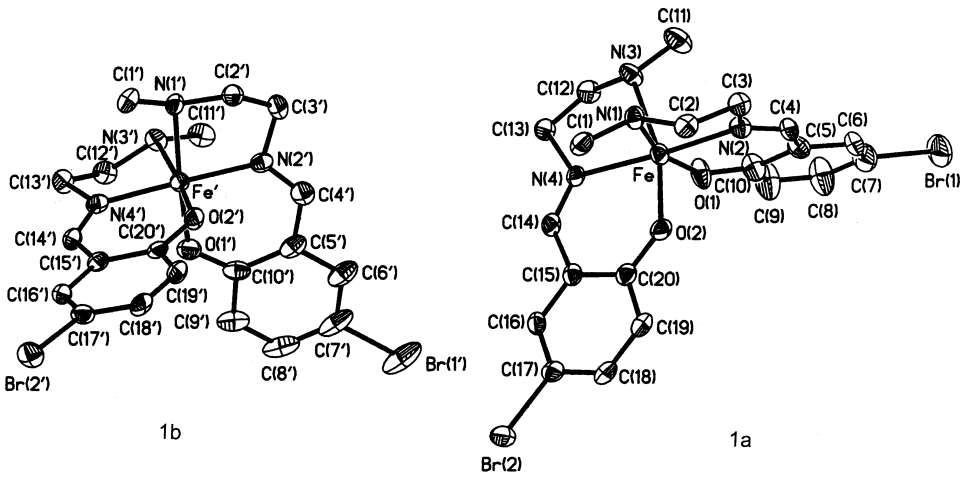

Fig. 1. Perspective view of complex **1** (**1a** is high-spin state and **1b** is low-spin state) with the atom numbering scheme. The anion ClO_4^- is omitted for clarity. Thermal ellipsoids are drawn at 50% probability level.

Magnetic Susceptibility, ESR and Mössbauer Spectra

The temperature dependences of $\chi_m T$ for complexes **1-3** are shown in Fig. 4. The Mössbauer spectra measured at 78 K for **1-3** are shown in Figs. 5-7.

As shown in Fig. 4, the values of $\chi_m T$ at 370 K for **1** and **2** are 4.28 cm^3 K mol^{-1} (μ_{eff} = 5.85 μ_B) and 3.68 cm^3 K mol^{-1} (μ_{eff} = 5.42 μ_B), respectively, lower than the spin only value 4.377 cm^3 K mol^{-1} (μ_{eff} = 5.92 μ_B) for S = 5/2. As the temperature is lowered the $\chi_m T$ values are gradually decreased to the value of 3.00 cm^3 K mol^{-1} for **1** and 1.36 cm^3 K mol^{-1} for **2** at 150 K, respectively. There is a "plateau" in the ($\chi_m T$ value vs. T in the range ca. 150-30 K for **1** and 130 K-20 K for **2**; this implies that the ratio of the mixed low-spin Fe(III) and high-spin Fe(III) states are without changes in this temperature range; it finally decreases abruptly to 1.58 cm^3 K mol^{-1} for **1** and 0.90 cm^3 K mol^{-1} for **2**, respectively, at 2 K. This behavior is unusual, because the $\chi_m T$ value vs. T curve shows three magnetic processes (first 370-150 K, 150-30 K, and < 30 K for **1**, 370-150 K, 130-20 K, and < 20 K) and the spin transition from high-spin to low-spin is incomplete in both complexes **1** and **2**. The fraction f_{HS} of the high-spin species was calculated at each temperature by using a simple additive property of magnetic susceptibilities as $f_{HS} = [\chi_m T - (\chi_m T)_{LS}]/[(\chi_m T)_{HS} - (\chi_m T)_{LS}]$. Here the values of pure HS and LS forms, $(\chi_m T)_{HS}$ and $(\chi_m T)_{LS}$, are taken from the experimental magnetic data. From this equation, the f_{HS} values of 0.55 for complex **1** at 150-30 K and 0.1 for complex **2** at 150-20 K were calculated. The value of $\chi_m T$ of complex **3** is 2.07 cm^3 K mol^{-1} (μ_{eff} = 4.07 μ_B) at 370 K, lower than that of the spin only value 4.377 cm^3 K mol^{-1} (μ_{eff} = 5.92 μ_B) for S = 5/2. As the temperature is lowered the $\chi_m T$ values are rapidly decreased to the values of 0.65 cm^3 K mol^{-1} (μ_{eff} = 2.28 μ_B) at 78 K and 0.35 cm^3 K mol^{-1} (μ_{eff} = 1.65 μ_B) at 2 K, respectively. The f_{HS} is calculated to be 0.10 at 78 K.

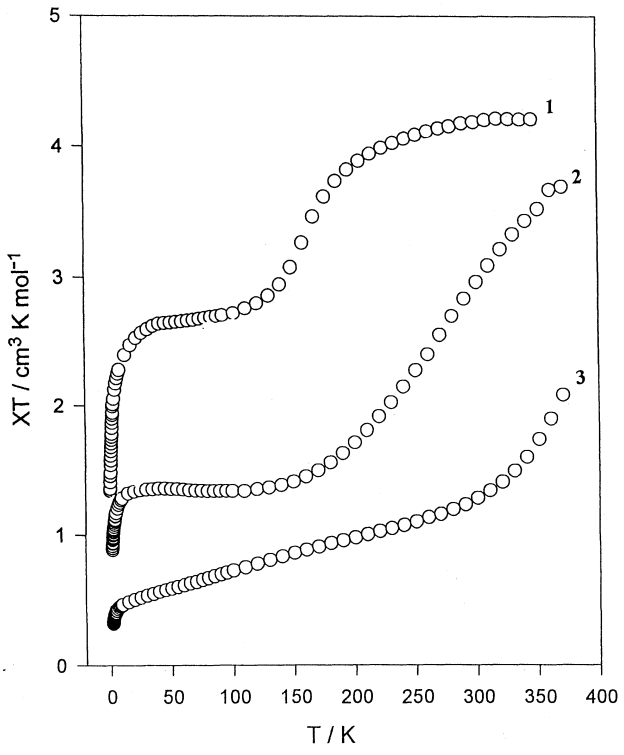

Fig. 4. Temperature dependence of $\chi_m T$ for complex **1**, **2**, and **3**.

The ESR spectrum of **1** at 77 K showed two broad absorptions around 0.15 and 0.33 T, the former being characteristic of high-spin Fe(III) species and the latter of low-spin Fe(III) species. ESR spectra at 77 K showed two absorptions at g_1 = 2.02, g_2 = 2.18 for **2** and g_1 = 1.98, g_2 = 2.19 for **3**, respectively, characteristic of low-spin Fe(III) species.

The broad Mössbauer absorption spectra at 300 K of **1** and **2** were observed which is characteristic of high-spin Fe(III) species; however, at 78 K the spectra (Figs. 5 and 6)

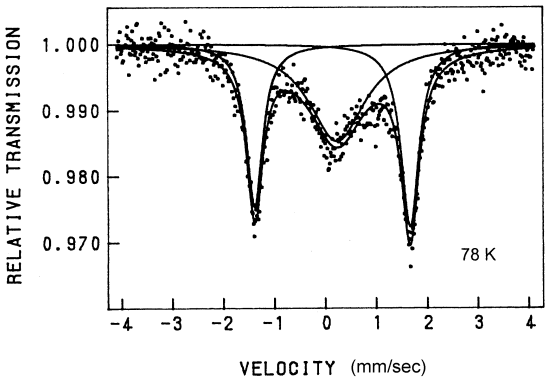

Fig. 5. Mössbauer spectra at 78 K for complex **1**. The solid line is plot with the fitted parameters reported in the text.

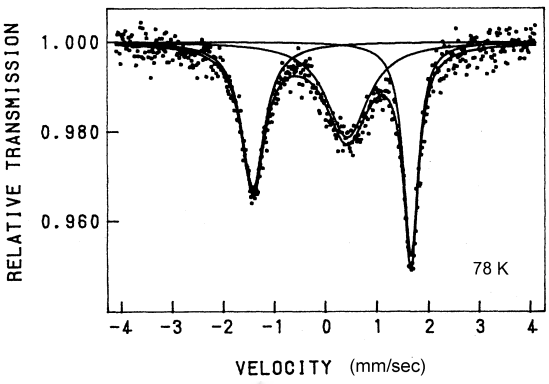

Fig. 6. Mössbauer spectra at 78 K for complex **2**.

with two doublets were observed, where the outer larger quadrupole doublet is low-spin isomer and the inside smaller quadrupole doublet is high-spin isomer. The population of high-spin isomer at 78 K was calculated to be 50% for **1** and 35% for **2** from the area of the Mössbauer absorption. The Mössbauer absorption spectra of **3** at 298 K and 78 K (see Fig. 7) showed two larger quadrupole doublets absorptions, where the outer quadrupole doublet is low-spin isomer and the inside quadrupole doublet is high-spin isomer. In addition, the f_{HS} ca. 0.30 calculated from the area of the Mössbauer absorption spectrum at 78 K for **3** is higher than 0.10 calculated from the magnetic susceptibilities measurements, implying that the recoiless fraction of high-spin species is not equivalent to that of the low-spin species.

Electronic Spectra and H_2O_2 Disproportionation

The absorption of UV-vis spectra of the complexes **1**-**3** measured at 300 K in methanol reveals the following transitions at 362, 548 and 680 nm for **1**, 365, 540 and 665 nm for **2**, and 347, 435, and 550 nm for **3**, respectively. The representative absorption spectra with one pyridine added in the solution for **2** is shown in Fig. 8. The absorption bands are assigned to salen-Fe(III) charge transfer transitions (LMCT) from p_π orbital of salen to d_{π^*} and d_{σ^*} of iron, respectively.[16-17] In addititon, it has been found that when pyridine was added, after 30 min there was no significant change that occurred in the electronic spectrum of the solution (see Fig. 8a). It should be also noted here that after 30s (b), 3 min.(c) and 6 min (d) the disproportionation of H_2O_2 in the methanol solution of the complexes **1**-**3** caused drastic changes in the 347-680 nm bands, the color of the solutions change to yellow, that is the disappearance of the LMCT bands which are characteristic of the dissociation of phenolate-Fe(III) bond.

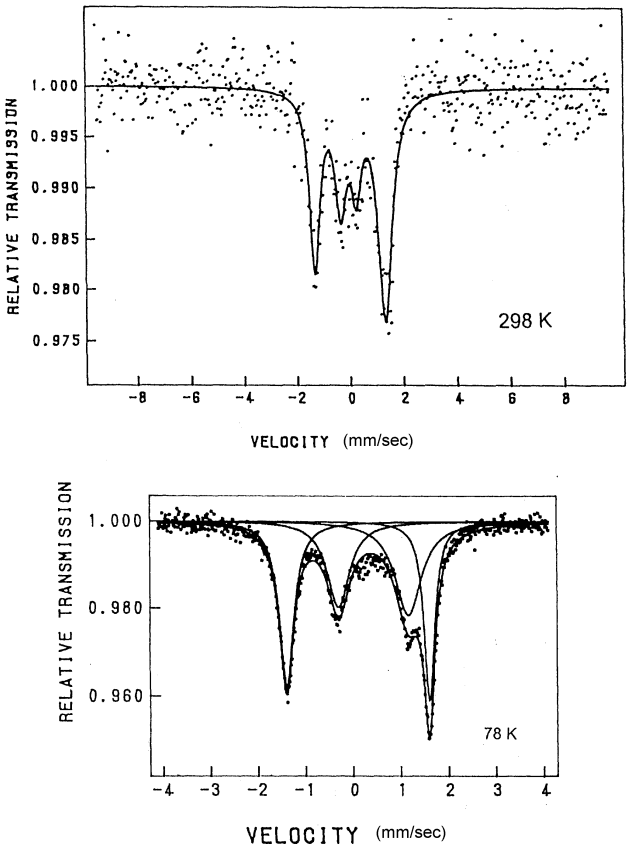

Fig. 7. Mössbauer spectra at 298 and 78 K for complex **3**.

Studies of H_2O_2 Disproportionation

The dependence of initial rates of H_2O_2 disproportionation was examined with varying concentration complexes **1**-**3**. In the first experiment, the hydrogen peroxide concentration was kept constant and the concentration of the complex was varied. Plots of the initial rate vs. catalyst concentration indicated that the reaction was first order in metal complex concentration. In a second experiment the catalyst concentration was kept constant and the H_2O_2 concentration

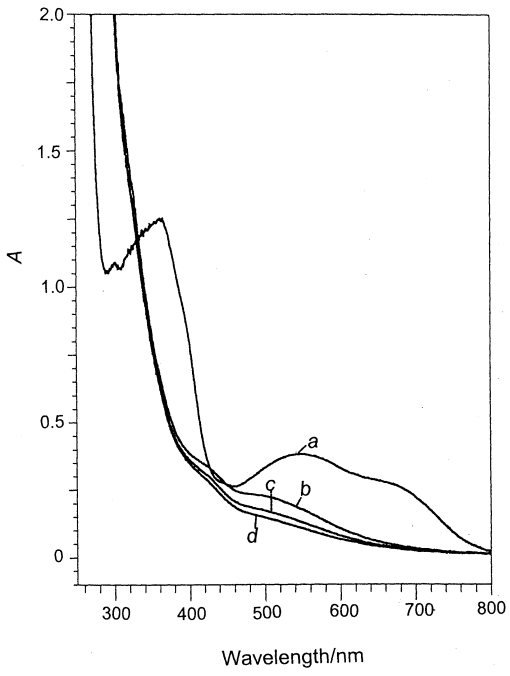

Fig. 8. Electronic spectrum for **2** in methanol solution (1.5×10^{-4} M) *a*, without addition of H_2O_2 *b*: 30 s. *c*: 3 min and *d*: 6 min after H_2O_2 (30%, 1 mL) added.

was varied. The initial rate depends linearly on the initial H_2O_2 concentration, as shown in Fig. 9. In the rate law (1) k_{obs} were calculated as 1.77 $dm^3\ mol^{-1}\ s^{-1}$ for **1**, 1.00 $dm^3\ mol^{-1}\ s^{-1}$ for **2**, and 1.23 $dm^3\ mol^{-1}\ s^{-1}$ for **3**.

$$\text{rate} = k_{obs}\,[H_2O_2]\,[\text{complex}] \quad (1)$$

The results of kinetics studies of catalase-like model complexes **1**-**3** just described above are similar to these of catalase-like hemerytherin model complexes with a $[Fe_2(\mu\text{-}O)(\mu\text{-}CH_3CO_2)_2]^{2+}$ core[18-19] that the initial rate of the reaction was first order in $[H_2O_2]$ concentration. At this stage, although the catalytic mechanism for interpretation for the present system is not known, however, here we adopted a possible catalytic cycle which is described as the known heme-type catalase.[20-22] In the heme catalases the peroxide reduction reaction $H_2O_2 + 2e^- + 2H^+ \rightarrow 2H_2O$ is accomplished by an Fe(III)-protoporphyrin IX center that generates compound **I**, formulated as a ferryl porphyrin π-cation radical $(O{=}Fe(IV)^+)$.[20-22] This species catalyses the peroxide oxidation reaction of $H_2O_2 \rightarrow O_2 + 2e^- + 2H^+$ in the case of heme peroxidases.[21]

The observed stimulatory effects of electron-rich pyridine on H_2O_2 decomposition in the present system could be explained by its general acid-base catalytic properties, which would facilitate proton transfers, and favor homolysis of the O-O bond by reducing the activation energy.[22]

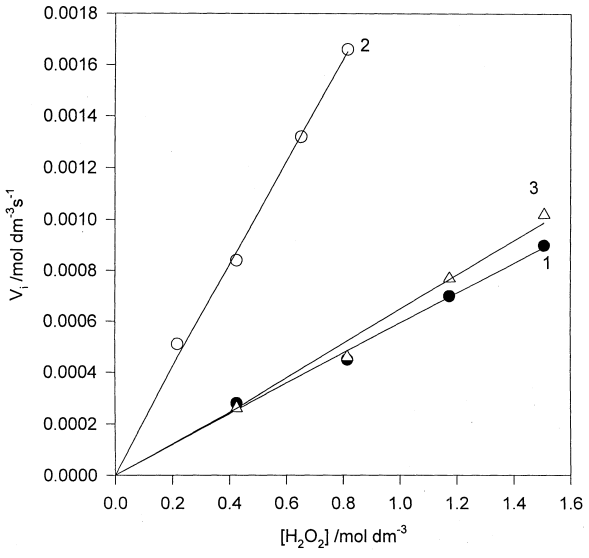

Fig. 9. Plots of the initial rate (V_i) of O_2 evolution as a function of $[H_2O_2]$ at 25° and pH = 7 in methanol solution of complex **1** (•), **2** (○), or **3** (Δ).

ACKNOWLEDGEMENTS

We thank the National Science Council of Taiwan for support of this research under Grant NSC-89-2113-M-032-008.

Received May 22, 2002.

Key Words

Iron(III) complexes; Structures; Magnetic properties; Spin crossover; Catalase.

REFERENCES

1. (a) Fita, I. A.; Silva, M.; Murthy, M. R. N.; Rossmann, M. G. *Acta. Cryst.* **1986,** *B42*, 497. (b) Fita, I.; Rossmann, M. G. *J. Mol. Biol.* **1985**, *185*, 21. (c) Vainshtein, B. K.; Melik-Adamyan, W. R.; Barynin, V. V.; Vagin, A. A.; Grebenko, A. I.; Borisov, V. V.; Bartels, K. S.; Fita, I.; Rossmann, M. G. *J. Mol. Biol*. **1986**, *188*, 49.
2. (a) Mauerer, B.; Crane, J.; Schuler, J.; Wieghardt, K.; Nuber, B. *Angew. Chem. Int. Ed. Engl*. **1993**, *32*, 289. (b) Ménage, S.; Vincent, J. M.; Lambeaux, C.; Fontecave, M. *J. Chem. Soc., Dalton Trans.* **1996**, 2081.
3. (a) Ito, S.; Okuno, T.; Matsushima, H.; Tokii, T.; Nishida, Y. *J. Chem. Soc., Dalton Trans*. **1996**, 4479. (b) Okuno, T.; Ito, S.; Ohba, S.; Nishida, Y. *J. Chem.Soc., Dalton Trans*. **1997**, 3547. (c) Nishino, S.; Hosomi, H.; Ohba, S.; Matsushima, H.; Tokii, T.; Nishida, Y. *J. Chem. Soc., Dalton Trans*. **1999**, 1509.
4. Chen, W. H.; Wei, H. H.; Lee, G. H.; Wang, Yu. *Polyhedron*. **2001**, *20*, 515.
5. (a) Sinn, E.; Sim, G.; Dose, E. V.; Tweedle, M. F.; Wilson, L. J. *J. Am. Chem. Soc.* **1978**, *100*, 3375. (b) Sim, P. G.; Sinn, E.; Petty, D. H.; Merril, C. L.; Wilson, L. J. *Inorg. Chem*. **1981**, *20*, 1213.
6. Haddad, M. S.; Lynch, M. W.; Federer, W. D.; Hendrickson, D. N. *Inorg. Chem.* **1981**, *20*, 123. (b) Federer, W. D.; Hendrickson, D. N. *Inorg. Chem*. **1984**, *23*, 3861. (c) Timken, M. D.; Hendrickson, D. N.; Sinn, E. *Inorg. Chem.* **1985**, *24* 3947.
7. (a) Matsumoto, N.; Kimoto, K.; Ohyoshi, A.; Maeda, Y. *Bull. Chem. Soc., Jpn.* **1984**, *57*, 3307. (b) Maeda, Y.; Takashima, Y.; Matsumoto, N.; Ohyoshi, A. *J. Chem. Soc., Dalton Trans*. **1986,** 1115. (c) Maeda, Y.; Oshio, H.; Takashima,Y.; Mikuriya, M.; Hidaka, M. *Inorg. Chem.* **1986**, *25*, 2958. (d) Oshio, H.; Toriumi, K.; Maeda, Y.; Takashima, Y. *Inorg. Chem*. **1991**, *30*, 4252.
8. Bernhardt, P. V.; Comba, P.; Hambley, T. W.; Lawrance, G.

A. *Inorg.Chem*. **1991**, *30,* 942.
9. (a) Conti, A. J.; Chadha, R. K.; Sena, K. M.; Rheingold, A. L.; Hendrickson, D. N. *Inorg. Chem*. **1993**, *32,* 2670. (b) Conti, A. J.; Kaji, K.; Nagano, Y.; Sena, K. M.; Yumoto, Y.; Chadha, R. K.; Rheingold, A. L.; Sorai, M.; Hendrickson, D. N. *Inorg. Chem.* **1993**, *32*, 2681.
10. Fukuya, M.; Ohba, M.; Motoda, K. I.; Matsumoto, N.; Okawa, H.; Meda, Y. *J. Chem. Soc., Dalton Trans*. **1993**, 3277.
11. Hernández-Molina, R.; Mederos, A.; Dominguez, S.; Gili, P.; Ruiz-Pérez, C.; Castiñeiras, A.; Solans, X.; Lloret, F.; Real, J. A. *Inorg. Chem.* **1998**, *37*, 5102.
12. Kahn, O. *Molecular Magnetism*; VCH: New York, 1993; p 3.
13. Sheldrick, G. M. *SHELXL-93.* Program for the Refinement of Crystal Structures; University of Gottingen, 1993.
14. (a) Calligaris, M.; Nardin, G.; Randaccio, L. *Coord. Chem. Rev.* **1972**, *7*, 385. (b) Oosterhuis, W. T. *Struct. Bonding* (Berlin). **1974**, *20*, 59.
15. Matsumoto, N.; Ohta, S.; Yoshimura, C.; Ohyoshi, A.; Kohata, S.; Okawa H.; Maeda, Y. *J. Chem. Soc., Dalton Trans.* **1985**, 2575.
16. (a) Viswanathan, R.; Palaniandavar, M. *J. Chem. Soc., Dalton Trans.* **1995**, 1259. (b) Viswanathan, R.; Palaniandavar, M.; Balasubramanian, T.; Prabakaran, P.; Thomas Muthiah, P. *Inorg. Chem.* **1998**, *37*, 3881.
17. Neves, A.; Rossi, L. M.; Vencato, I.; Haase, W.; Werner, R. *J. Chem. Soc., Dalton Trans.* **2000**, 707.
18. (a) Mauerer, B.; Crane, J.; Schuler, J.; Wieghardt, K.; Nuber, B. *Angew. Chem. Int. Ed. Engl.* **1993**, *32*, 289. (b) Ménage, S.; Vincent, J. M.; Lambeaux, C.; Fontecave, M. *J. Chem. Soc., Dalton Trans*. **1996**, 2081.
19. (a) Ito, S.; Okuno, T.; Matsushima, H.; Tokii, T.; Y. Nishida, Y. *J. Chem. Soc., Dalton Trans.* **1996**, 4479. (b) Okuno, T.; Ito, S.; Ohba, S.; Nishida, Y. *J. Chem. Soc., Dalton Trans.* **1997**, 3547. (c) Nishino, S.; Hosomi, H.; Ohba, S.; Matsushima, H.; Tokii, T.; Nishida, Y. *J. Chem. Soc., Dalton Trans.* **1999**, 1509.
20. Sawyer, D. T. *Oxygen Chemistry*; Oxford University Press: New York, 1991; p 21.
21. Xie, K. Y.; Dophin, D. *Handbook of Metal-Ligand Interactions in Biological Fluids*; G. Berthon, Ed.; Marcel Dekker: New York, 1995; pp 339-351.
22. Dawson, J. H. *Science.* **1988**, *240*, 433. (b) Sono, M.; Roach, M. P.; Coulter, E. D.; Dawson. H. *Chem. Rev.* **1996**, *96*, 2841.